Cellulose (2015) 22:3251–3260
DOI 10.1007/s10570-015-0702-3

ORIGINAL PAPER

Improvement of the electromechanical performance of carboxymethylcellulose-based actuators by graphene nanoplatelet loading

Okan Ozdemir · Ramazan Karakuzu · Mehmet Sarikanat · Yoldas Seki · Emine Akar · Levent Cetin · Ozgun Cem Yilmaz · Kutlay Sever · Ibrahim Sen · Baris Oguz Gurses

Received: 11 March 2015 / Accepted: 6 July 2015 / Published online: 17 July 2015

Abstract In this article, the effects of graphene loading (0.1, 0.2, 0.3 wt%) on both the electromechanical and mechanical properties of carboxymethylcellulose (CMC)-based actuators were investigated. CMC-based graphene-loaded actuators were prepared by using 1-butyl-3-methylimidazolium bromide. The synthesized graphene-loaded actuators were characterized by Fourier transform infrared, X-ray diffraction analysis, thermogravimetric analysis, scanning electron microscopy, and tensile tests. Electromechanical properties of the actuators were obtained under DC excitation voltages of 1, 3, 5, and 7 V with a laser displacement sensor. According to the obtained results, the ultimate tensile strength of CMC-based actuators containing 0.3 wt% graphene was higher than that of unloaded actuators by approximately 72.8 %. In addition, the Young's modulus value of the graphene-loaded actuators increased continuously with increasing graphene content. Under a DC excitation voltage of 5 V, the maximum tip displacement of 0.2 wt% graphene-loaded actuators increased by about 15 % compared to unloaded actuators.

Keywords Electromechanical properties · Carboxymethylcellulose · Smart materials · Mechanical properties · Graphene

Introduction

Electroactive polymers (EAPs) have been widely developed for many applications owing to their unique sensing and actuation advantages. Among these

O. Ozdemir (✉) · R. Karakuzu
Department of Mechanical Engineering, The Graduate School of Natural and Applied Sciences, Dokuz Eylul University, Izmir, Turkey
e-mail: ozdemir.okan@deu.edu.tr

M. Sarikanat · B. O. Gurses
Department of Mechanical Engineering, Ege University, Izmir, Turkey

Y. Seki · E. Akar
Department of Chemistry, Dokuz Eylul University, Izmir, Turkey

E. Akar
Department of Bioengineering, Çanakkale Onsekiz Mart University, Çanakkale, Turkey

L. Cetin
Department of Mechatronics Engineering, İzmir Katip Çelebi University, Izmir, Turkey

O. C. Yilmaz
Department of Mechatronics Engineering, The Graduate School of Natural and Applied Sciences, Dokuz Eylul University, Izmir, Turkey

K. Sever
Department of Mechanical Engineering, İzmir Katip Çelebi University, Izmir, Turkey

I. Sen
Department of Biocomposites, The Graduate School of Natural and Applied Sciences, İzmir Katip Çelebi University, Izmir, Turkey

polymers, ionic polymer metal composites (IPMCs), which show bending behaviors to applied low voltages, are candidate materials for applications in smart structures, artificial muscles, and robotic systems (Bar-Cohen 2012; Kikuchi and Tsuchitani 2009; Shahinpoor et al. 1998; Shahinpoor and Kim 2001).

Cellulose, which is the most abundant biomolecule on earth, can be commonly used to fabricate ionic polymer actuators because of mechanical endurance, hydrophilicity, biocompatibility, and capability of broad chemical modification (Murphy and Wudl 2010; Qiu and Hu 2013). Moreover, it has drawn considerable interest and encouraged researchers to develop smart materials based on cellulose in the last 2 decades (Ana Baptista et al. 2013). Kim et al. (2006) produced bending actuator-based cellulose paper and revealed the actuation phenomenon of the actuator. However, dissolution of cellulose in water is difficult because of the crystalline structure. Cellulose can be dissolved by some solvents; however, they are toxic, volatile, and unstable during the dissolution processing (Cao et al. 2009; Kim and Kim 2013). Carboxymethylcellulose (CMC), which can be dissolved in water, is one of the cellulose derivatives that can also be used as a smart material (Haldorai and Shim 2014; Qiu and Hu 2013; Shang et al. 2008). Besides, using ionic liquid (IL) is the other successful alternative method to overcome the problem regarding the dissolution of cellulose and its derivatives (Hua et al. 2014; Muzart 2006; Patil and Sasai 2008). Also, it there are many studies using ILs in order to produce an actuator (Edgar et al. 2001; Fischer et al. 2002; Swatloski et al. 2002). Among the ionic liquids (ILs), 1-butyl-3-methylimidazolium bromide (BMIMBr) melts at a relatively low temperature and has been used in many application areas (Akbari and Heydari 2012; Goswami et al. 2012; Yang et al. 2014; Zare et al. 2011). In our previous study, we investigated the effect of polyethylene glycol (PEG) on the electromechanical properties of a CMC-based actuator created with BMIMBr ionic liquid (Ozdemir et al. 2015).

Graphene, which is a stable 2D one-atom-layer material, shows excellent properties, i.e., good electrical conductivity and mechanical strength, a large surface area and superior performance (Huang et al. 2012; Lee et al. 2008; Novoselov et al. 2004; Xia et al. 2009). Feng et al. (2012) emphasized that graphene loading enhanced the electrical and mechanical properties. Zhao et al. (2013) also investigated the effects of graphene loading into smart materials and found that graphene-loaded actuators can be used as sensors, switches and artificial muscles.

In the present study, we attempted to improve the actuation characteristic of CMC-based actuators by using three different graphene loadings (0.1, 0.2, 0.3 wt%). Selected ratios were used in order to investigate the optimum actuation performance. It is also difficult to distribute the higher graphene content homogeneously. Characterization of graphene-loaded CMC-based films was performed by thermogravimetric analysis (TGA), X-ray diffraction analysis (XRD), Fourier transform infrared analysis (FTIR), scanning electron microscopy (SEM) and tensile tests. Besides, the electromechanical behavior of the actuators was determined under different DC excitation voltages.

Experiments

Materials

Carboxymethylcellulose sodium salt with low viscosity [C5678-500G; degree of substitution (DS): 0.65–0.90 and molecular weight: 90 kDa], 1-butyl-3-methylimidazolium bromide (BMIMBr) and PEG (average mol. wt. 1450 g/mol) were supplied by Sigma-Aldrich. Graphene nanoplatelets (Gr), having an average particle diameter of 50–100 nm and thickness of approximately 5–10 μm, were purchased from Grafen Kimya Sanayi A.Ş.

Preparation of CMC-based IPMC actuators

Sodium carboxymethylcellulose (NaCMC) (1.44 g) was dissolved in 14.4 ml distilled water at room temperature. Afterwards, 3.21 g BMIMBr was added to the prepared solution. The solution was placed into the hot water bath (90–95 °C) and stirred until a homogeneous mixture was obtained. The bending behavior of an IPMC actuator is known to depend on the brittle characteristic and weak mechanical property of the actuators. In order to improve these undesirable properties, Pang et al. (2013) suggested the plasticization method. PEG can be used as a plasticizer to enhance the mechanical properties of the actuator (Cai and Kim 2010). Since the optimal amount of PEG was found to be 1.5 g (Ozdemir et al.

2015), after dissolution of BMIMBr, 1.5 g of PEG was added to this mixture. Gr with fractions of 0.1, 0.2 and 0.3 wt% total mass material was dispersed in the solution by using an ultrasonic homogenizer. In this study, graphene-loaded CMC-based films were termed CMC–Br–0.1Gr, CMC–Br–0.2Gr and CMC–Br–0.3Gr. The mixture was cast in a petri dish and dried at room temperature for 24 h. Finally, IPMC actuators were prepared by coating gold leaf (0.14 μm, L.A. Gold Leaf) on each side of the films.

Thermogravimetric analysis (TGA)

The effect of Gr loading on the thermal stability of CMC–Br films was investigated by thermogravimetric analysis (Perkin-Elmer Pyris TGA). The analyses were conducted at a heating rate of 10 °C/min from 30 to 600 °C under nitrogen atmosphere.

FTIR analysis

FTIR analysis of the samples was performed using an FTIR Perkin-Elmer Spectrum BX-II. The spectra were recorded with the sum of 25 scans at a resolution of 4 cm^{-1} in the range of 4000–400 cm^{-1}.

X-ray diffraction (XRD)

Crystalline structures of the samples were analyzed using a Philips X-Pert Diffractometer. Ni-filtered Cu Kα radiation ($\lambda = 1.54$ Å) generated at a voltage of 45 kV and current of 40 mA was utilized with a time per step of 10 s and scan step size of 0.03°.

Scanning electron microscope (SEM) observations

The surface morphologies of the CMC–Br- and Gr-loaded CMC–Br samples were examined using a high-resolution scanning electron microscope (FEI Quanta FEG 250). The images were taken at an accelerating voltage of 5 kV. The gold sputtering of the samples was performed using the plasma sputtering technique.

Tensile tests

In order to determine the mechanical properties, tensile tests, with a crosshead speed of 0.1 mm/min, were conducted using a universal testing machine with a load cell capacity of 100 N. The sample dimensions were 10 × 40 mm.

Electroactive properties

The electromechanical behavior of CMC-based actuators was investigated under DC voltages of 1, 3, 5 and 7 V. Data acquisition hardware (NI-PXI 7854R) and a buffer circuit were utilized as the signal source. The maximum tip displacements of the actuators were measured by a KEYENCE LK-51 laser displacement sensor. Each test was repeated at least three times, and average values and standard deviations of the films were calculated.

Tensile tests and the maximum tip displacement of the films were determined at ambient temperature (24 °C). The relative humidity level was measured as 45 %.

Results and discussions

Thermogravimetric analysis

TGA curves of CMC–Br, CMC–Br–0.1Gr, CMC–Br–0.2Gr, and CMC–Br–0.3Gr are presented in Fig. 1. The mass loss up to 110 °C, initial decomposition temperature (T_i), maximum decomposition temperature (T_{max}), final decomposition temperature (T_f), mass loss up to T_{max}, and mass loss up to 600 °C are reported in Table 1. The decomposition of Gr-loaded and -unloaded samples took place in two steps. A small mass loss (8.5–12.5 %) for the first decomposition step and a more significant mass loss (56.4–58 %) for the second step (including the first step) were observed. The mass loss for the first step was probably due to evaporation of bound water. The greater amount of water may affect the actuation behavior positively to some extent, especially at low voltage values. After Gr loading, the mass loss up to 110 °C increased. The mass loss for the second decomposition step was ascribed to the degradation of the side chain and loss of CO_2 of CMC (El-Sayed et al. 2011). Also an increase in Gr loading did not lead to any variation in the maximum decomposition temperature. As can be seen from Table 1, while Gr loadings of 0.1 and 0.2 wt% increased the initial decomposition temperature, Gr loading of 0.3 wt%

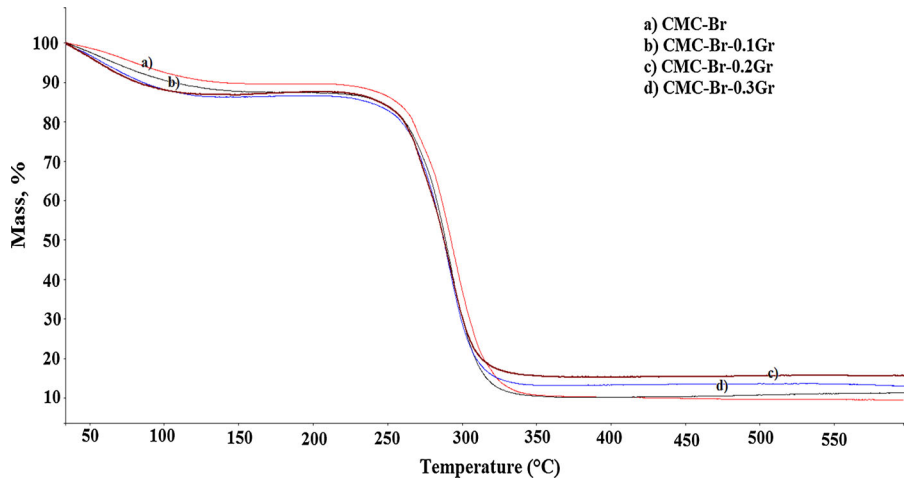

Fig. 1 TGA curves for the CMC-based films

Table 1 TGA results for the CMC-based films

Sample	Mass loss up to 110 °C (%)	$T_{initial}$ (°C)	T_{max} (°C)	T_{final} (°C)	Mass loss up to T_{max} (%)	Mass loss up to 600 °C (%)
CMC–Br	8.5	206	296	371	56.4	90.4
CMC–Br–0.1Gr	10.3	212	292	366	55.8	88.7
CMC–Br–0.2Gr	12.3	212	292	370	56.7	84.2
CMC–Br–0.3Gr	12.5	202	292	353	58.0	86.9

decreased it. After Gr was loaded into the samples, their mass loss in the 30–600 °C range decreased considerably. Therefore, it can be noted that Gr loading into the CMC, ionic liquid and PEG mixture increased the thermal decomposition residues observed because of the nonvolatile carbonaceous material. In addition, both the Gr-loaded and -unloaded actuators were thermally stable up to 200 °C.

FTIR analysis

The FTIR spectra of CMC–Br (without PEG), CMC–Br, CMC–Br–0.1Gr, CMC–Br–0.2Gr and CMC–Br–0.3Gr are shown in Fig. 2. The peaks at around 3400, 2960, 1610 and 1070 cm^{-1} belong to the hydroxyl group (–OH), asymmetric $–CH_2$, carboxyl group (–COO) and $>CH–O–CH_2$ group of sodium carboxymethylecellulose, respectively (Akar et al. 2012; Biswal and Singh 2004; Chai and Isa 2013; Habibi 2014).

The characteristic peaks at around 3145 and 3091, 2959 and 2872, 1613, 1573 and 1167 cm^{-1} are attributed to the imidazole ring (C–H), aliphatic C–H, O–H bending, imidazole ring, imidazole H–C–C and H–C–N bending of BMIMBr, respectively (Rajkumar and Ranga Rao 2008; Ranga Rao et al. 2009).

The methylene group of PEG exhibits an absorption peak at 2873 cm^{-1}. The vibration peak at around 1462 cm^{-1} is due to the binding vibration of the $–CH_2$ group. The absorption peaks at about 950 and 842 cm^{-1} are due to the C–C stretching (Polu and Kumar 2011; Polu et al. 2011). As shown in the spectrum of CMC–Br, the existence of these peaks, especially at 950 cm^{-1}, verified the PEG component in CMC–Br film.

The loading of Gr at different fractions into CMC–Br–PEG shifted the absorption bands from 3443, 2959, 1627 cm^{-1} and 1346 to 3441, 2957, 1629 and 1348 cm^{-1}, respectively. Very small shifts were observed because of weak secondary attractive forces between graphene layers and other components.

X-ray diffraction (XRD) analysis

X-ray diffraction curves of the CMC-based samples are depicted in Fig. 3. The characteristic diffraction peak for CMC occurs at $2\theta = 19.82°$. The amorphous

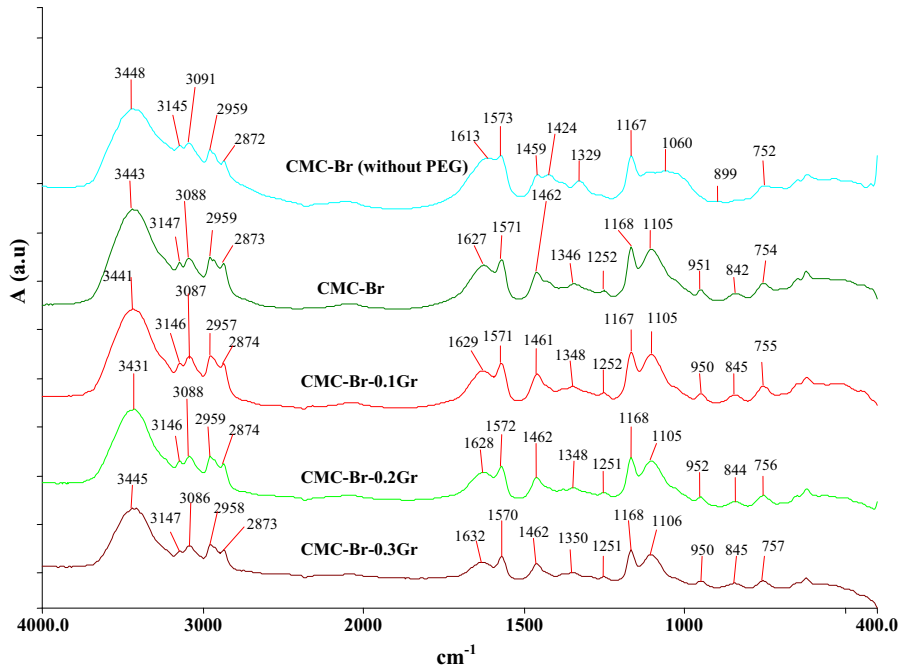

Fig. 2 FTIR spectrum of the CMC-based actuators

nature of CMC can be seen with a broad peak at $2\theta = 20°$ (Ravikiran et al. 2014). After loading of CMC into the BMIMBr (without PEG), the characteristic diffraction peak shifted to $2\theta = 22.70°$. The characteristic diffraction peak of the Cel–Br (with PEG) actuator was observed at approximately $2\theta = 23.39°$, probably indicating the presence of PEG. According to Bell et al. (2014), the XRD pattern of PEG showed two peaks at $2\theta = 19.2°$ and 23.4°. After Gr was loaded into CMC, the main characteristic peak of Gr did not appear distinctly in the patterns of Gr-loaded CMC–Br samples. Namely, one can note that the matrix effect still is dominant. Wojtoniszak et al. (2012) indicated that the characteristic peak at $2\theta = 26.475°$ in graphite appeared. However, no peak regarding Gr was observed in this range, as shown in the XRD spectra of CMC–Br–0.1Gr, CMC–Br–0.2Gr and CMC–Br–0.3Gr. This may be attributed to the good dispersion of Gr into the CMC matrix. The decrease in intensity and change in 2θ values show that a new type of crystallite was created in the amorphous region (Jung et al. 2011).

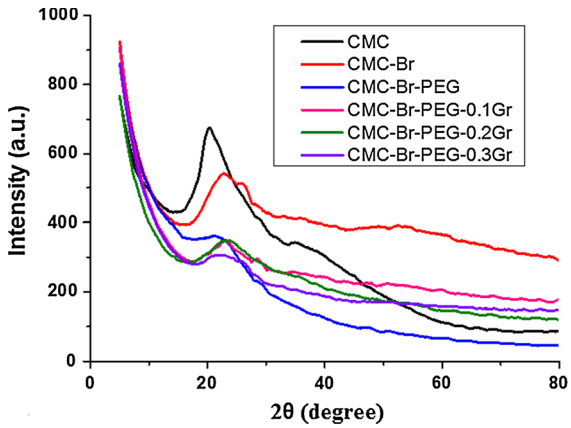

Fig. 3 XRD patterns of the CMC-based actuators

Scanning electron microscope (SEM) analysis

The surface morphologies of CMC–Br–0.1Gr, CMC–Br–0.2Gr and CMC–Br–0.3Gr films were investigated by scanning electron microscope (SEM). The micrographs of the samples are depicted in Fig. 4a–d. Figure 4a shows that CMC particles were dispersed on the nano and micro scales and distributed nearly homogeneously in the BMIMBr and PEG mixture. After Gr loading in the fractions of 0.1, 0.2 and 0.3 wt%, CMC particles could not be seen clearly except for 0.1 wt% Gr loading. CMC particles were well dispersed, and a homogeneous surface was obtained (Fig. 4b). On the other hand, some

agglomerated CMC particles were observed in the higher Gr loadings. This may be due to the fact that higher Gr loadings decreased the dispersion of CMC particles in the mixture of BMIMBr and PEG. Therefore, the surfaces of the Gr-loaded films were rougher compared to the unloaded films (Fig. 4c, d).

Tensile tests

The weak characteristic of CMC-based films is a major problem that limits the usage of films as an actuator, because if the films are not strong enough, they might be damaged when subjected to voltages or not exhibit good actuation performance. Hence, this problem should certainly be eliminated. In this context Jung et al. (2011) pointed out that the addition of graphene to the polymer may alter the static microphase morphology of the polymer, resulting in improved tensile strength accompanied by an increase in strain.

Young's modulus or the modulus of elasticity, which is used to characterize materials, can be defined as the slope of the stress-strain curve in the elastic region. Table 2 shows the effect of Gr loading on the tensile strength and Young's modulus values of CMC–BMIMBr-based films. The tensile strengths of Gr-loaded CMC–Br films were higher than those of unloaded counterparts. Moreover, the tensile strengths of Gr-loaded CMC–Br films increased with increasing Gr content, and the highest tensile strength was found for CMC–Br–0.3Gr. The tensile strength was increased from 12.24 MPa for CMC–Br to 21.15 MPa for the CMC–Br–0.3Gr. Thus, the tensile strength of CMC–Br increased by about 72.8 % after a Gr of 0.3 wt% was loaded. Our results showed a similar trend to those in the study of Jung et al. (2011). Table 2 shows that Gr-loaded CMC–Br films have higher Young's modulus values than CMC–Br film. Besides, the Young's modulus values for Gr-loaded CMC–Br films increased continuously with increasing Gr content. For CMC–Br,

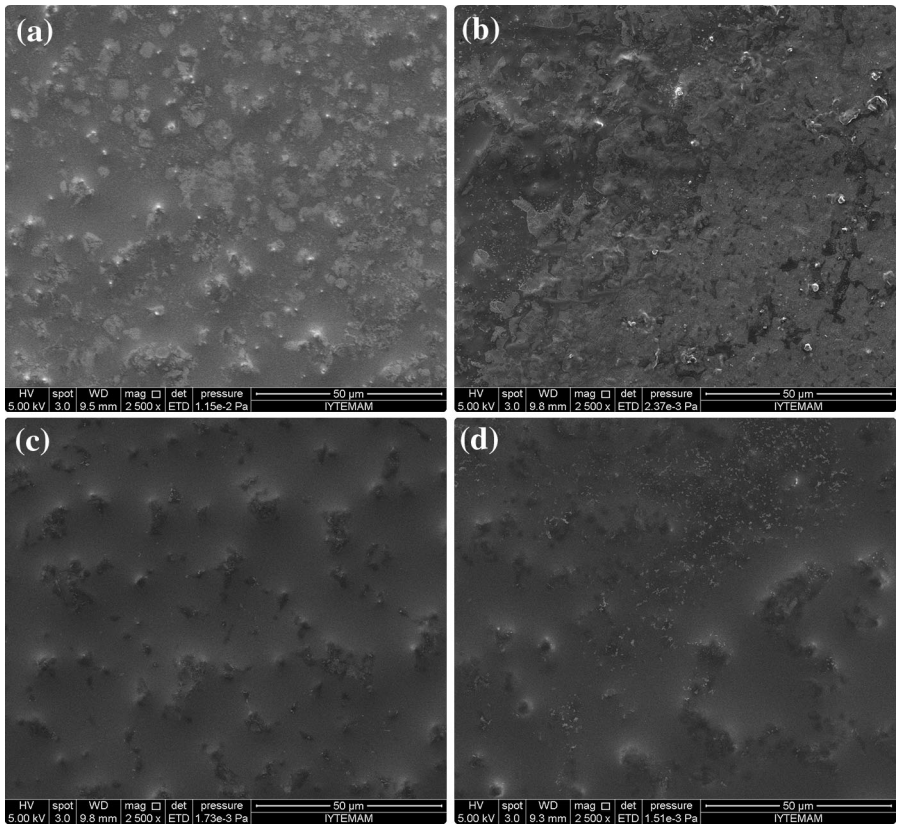

Fig. 4 SEM images of **a** CMC–Br, **b** CMC–Br–0.1Gr, **c** CMC–Br–0.2Gr and **d** CMC–Br–0.3Gr films

Table 2 Tensile test results of the CMC-based films

Sample name	Tensile strength (MPA)	Young's modulus (GPa)
CMC–Br	12.24 ± 0.42	0.24 ± 0.05
CMC–Br–0.1Gr	15.68 ± 0.31	0.28 ± 0.03
CMC–Br–0.2Gr	18.45 ± 0.24	0.34 ± 0.01
CMC–Br–0.3Gr	21.15 ± 0.47	0.42 ± 0.04

the Young's modulus obtained was 0.24 GPa. After 0.3 wt% Gr was loaded into CMC–Br–PEG, the Young's modulus value increased to 0.42 GPa. In other words, the increase in the Young's modulus value was about 75 % compared to that of CMC–Br films. These results may be attributed to the significant mechanical properties of Gr such as high tensile strength and high Young's modulus values (Nieto et al. 2012). Besides, the large surface area of Gr suggests significant improvement in the mechanical properties of the nanocomposites (Ahmad et al. 2015).

Electroactive properties

Electromechanical performances of Gr-loaded (0.1, 0.2, 0.3 wt%) CMC–Br films were studied under DC excitation voltages of 1, 3, 5 and 7 V. The tip displacements of the actuators were measured with a contactless laser displacement measurement system. The maximum tip displacement measurements were performed at a distance of 110 mm from the fixed end of the cantilever configuration. The time responses of the tip displacement of the samples are given in Fig. 5.

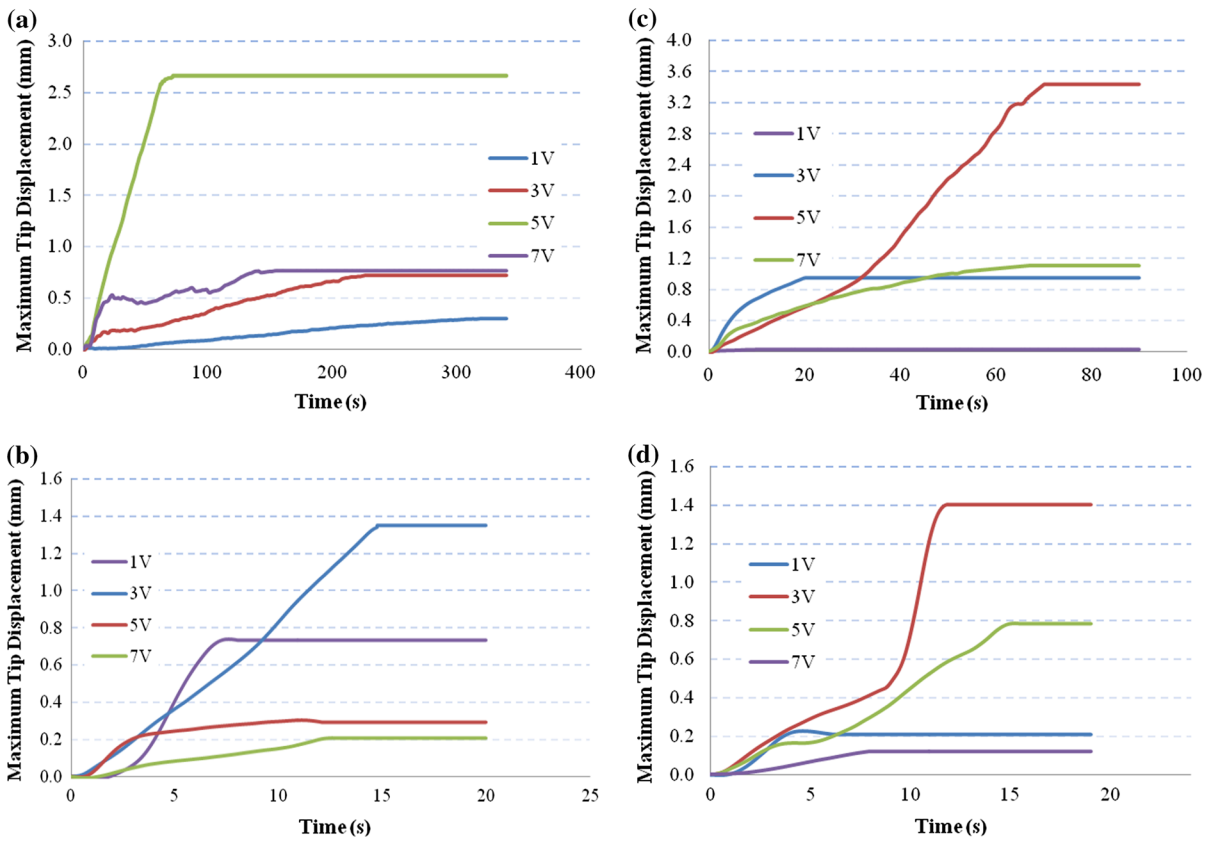

Fig. 5 The time responses of the tip displacement of the **a** CMC–Br, **b** CMC–Br–0.1Gr, **c** CMC–Br–0.2Gr and **d** CMC–Br–0.3Gr actuators

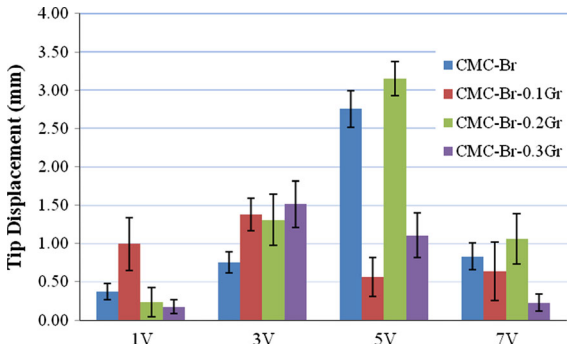

Fig. 6 Maximum tip displacement of gold-coated actuators with different Gr loadings

All acquired response curves are in an exponential form and have no back relaxation. Therefore, the final value of the tip displacements were considered the maximum tip displacement values of the actuator samples. These maximum values, given in Fig. 6 and Table 3, were used to evaluate the electromechanical performances of the actuator.

When the best performances of the actuator samples (the highest value in each row of Table 3) are considered, it can be seen that Gr loading increased the maximum tip displacement with respect to the unloaded actuator sample. The CMC–Br and CMC–Br–0.2Gr actuator samples have similar characteristics. Their maximum tip displacements increased when the excitation voltage increased from 1 to 5 V, but decreased when the excitation voltage increased from 5 to 7 V. It should also be noted that significant tip motions were observed for these two actuators at 7-V excitation voltage. On the other hand, Fig. 6 shows that the actuator sample with 0.2 wt% Gr loading has a very similar maximum tip displacement versus tip displacement curve to the unloaded actuator.

There are few studies on the maximum tip displacement of cellulosic films produced by dissolving cellulose and/or carboxymethylcellulose in BMIMBr ionic liquid, which makes direct comparisons with the our work challenging. Most of the fabrication parameters, i.e., type of ionic liquid, coating materials and coating method of the electrodes, and applied voltages in other studies differ significantly from our study. Sen et al. (2015) performed a similar study on IPMC actuators. They found that the maximum tip displacement of actuators increased with graphene loading up to 0.2 wt%. Besides, the maximum tip displacement of cellulose-based actuator containing graphene particles with fraction of 0.25 wt% was observed as 2.2 mm under DC voltage of 3 V. On the other hand, the maximum tip displacement of their actuators was determined as 0.5 mm under DC voltage of 5 V. When the maximum tip displacements in all voltages are considered, our current actuator has better characteristics than the actuators prepared by Sen et al. (2015) under DC voltages of 1, 5 and 7 V.

Eventually, the experimental results showed that the Gr loading into CMC-based samples improved the actuator performances. The highest improvement in maximum tip displacement was observed for CMC–Br–0.1Gr and CMC–Br–0.3Gr at approximately 100 % at excitation voltage of 3 V. When the actuators were excited with 5 V, it was observed that 0.2 wt% Gr loading increased the maximum tip displacement by about 15 % compared to the unloaded actuator.

Conclusion

In this study, CMC−Br-based actuators were fabricated using CMC, BMIMBr and PEG. The electromechanical behaviors of CMC–Br-based actuators were determined through a series of experiments. In order to improve the electromechanical behavior, three different weight percentages of Gr were loaded into the CMC–Br films. The mechanical, thermal and chemical characterizations of CMC–Br–Gr-based films were performed. It was observed that the tensile strength and Young's modulus values increased continuously with increasing Gr content. Loading BMIMBr, PEG and Gr into CMC affected the chemical structure of CMC and

Table 3 Maximum tip displacement of the CMC-based actuators (mm)

Sample name	1 V	3 V	5 V	7 V
CMC–Br	0.38 ± 0.11	0.75 ± 0.14	2.75 ± 0.23	0.83 ± 0.18
CMC–Br–0.1Gr	1.00 ± 0.35	1.38 ± 0.21	0.56 ± 0.26	0.63 ± 0.38
CMC–Br–0.2Gr	0.24 ± 0.19	1.31 ± 0.34	3.15 ± 0.22	1.06 ± 0.33
CMC–Br–0.3Gr	0.18 ± 0.09	1.52 ± 0.30	1.11 ± 0.29	0.23 ± 0.11

caused the formation of new bands. XRD analysis showed that the main characteristic peak of Gr was not seen clearly in the Gr-loaded actuators. Considering the thermal characteristics, it can be inferred that Gr loading into CMC-based actuators increased the thermal decomposition residues observed because of the nonvolatile carbonaceous material. Besides, there was no significant effect of Gr loading on the maximum decomposition temperature. When actuator responses to electrical stimuli were considered, it was observed that the loading of 0.2 wt% Gr into CMC–Br increased the maximum tip displacements of the CMC–Br actuator by about 15 % for an excitation voltage of 5 V. Moreover, the loadings of 0.1 and 0.3 wt% Gr into CMC–Br increased the maximum tip displacements of the CMC–Br actuator by about 100 % for an excitation voltage of 3 V.

Acknowledgments This study was supported by TUBITAK—The Scientific and Technological Research Council of Turkey, project no. 111M643.

References

Ahmad SR, Young RJ, Kinloch IA (2015) Raman spectra and mechanical properties of graphene/polypropylene nano composites. Int J Chem Eng Appl. doi:10.7763/IJCEA.2015.V6.440

Akar E, Altınışık A, Seki Y (2012) Preparation of pH-and ionic-strength responsive biodegradable fumaric acid cross-linked carboxymethyl cellulose. Carbohydr Polym 90:1634–1641

Akbari J, Heydari A (2012) Synthesis of Mn_3O_4 nanoparticles with controlled morphology using ionic liquid. Curr Nanosci 8:398–401

Baptista A, Ferreira I, Borges J (2013) Cellulose-based bio-electronic devices. In: van de Ven T, Godbout L (eds) Cellulose—medical, pharmaceutical and electronic applications. doi:10.5772/56721

Bar-Cohen Y (2012) Electroactive polymer (EAP) as actuators for biomimetic applications. In: Proceedings of the ASME international mechanical engineering congress and exposition (IMECE 2010) vol 9, pp 655–660

Bell SSJ, Geethanjali R, Subhashini S (2014) Synthesis and characterization of polyethylene glycol-G-Arginine and its corrosion—inhibition behaviour on mild steel. J Environ Nanotechnol 3:23–29

Biswal D, Singh R (2004) Characterisation of carboxymethyl cellulose and polyacrylamide graft copolymer. Carbohydr Polym 57:379–387

Cai Z, Kim J (2010) Bacterial cellulose/poly(ethylene glycol) composite: characterization and first evaluation of biocompatibility. Cellulose 17:83–91. doi:10.1007/s10570-009-9362-5

Cao Y, Wu J, Zhang J, Li HQ, Zhang Y, He JS (2009) Room temperature ionic liquids (RTILs): a new and versatile platform for cellulose processing and derivatization. Chem Eng J 147:13–21. doi:10.1016/j.cej.2008.11.011

Chai M, Isa M (2013) The oleic acid composition effect on the carboxymethyl cellulose based biopolymer electrolyte. J Crystal Process Technol 3:1

Edgar KJ, Buchanan CM, Debenham JS, Rundquist PA, Seiler BD, Shelton MC, Tindall D (2001) Advances in cellulose ester performance and application. Prog Polym Sci 26:1605–1688. doi:10.1016/S0079-6700(01)00027-2

El-Sayed S, Mahmoud KH, Fatah AA, Hassen A (2011) DSC, TGA and dielectric properties of carboxymethyl cellulose/polyvinyl alcohol blends. Phys B 406:4068–4076. doi:10.1016/j.physb.2011.07.050

Feng YY, Zhang XQ, Shen YT, Yoshino K, Feng W (2012) A mechanically strong, flexible and conductive film based on bacterial cellulose/graphene nanocomposite. Carbohydr Polym 87:644–649. doi:10.1016/j.carbpol.2011.08.039

Fischer S, Thummler K, Pfeiffer K, Liebert T, Heinze T (2002) Evaluation of molten inorganic salt hydrates as reaction medium for the derivatization of cellulose. Cellulose 9:293–300. doi:10.1023/A:1021121909508

Goswami D, Chattopadhyay A, Sharma A, Chattopadhyay S (2012) [bmim][Br] as a solvent and activator for the Ga-mediated barbier allylation: direct formation of an N-heterocyclic carbene from Ga metal. J Org Chem 77:11064–11070. doi:10.1021/Jo3020775

Habibi N (2014) Preparation of biocompatible magnetite-carboxymethyl cellulose nanocomposite: characterization of nanocomposite by FTIR, XRD, FESEM and TEM. Spectrochim Acta Part A Mol Biomol Spectrosc 131:55–58

Haldorai Y, Shim JJ (2014) Chemo-responsive bilayer actuator film: fabrication, characterization and actuator response. New J Chem 38:2653–2659. doi:10.1039/C4nj00014e

Hua L et al (2014) Immobilization of polyoxometalate-based ionic liquid on carboxymethyl cellulose for epoxidation of olefins. New J Chem 38:3953–3959. doi:10.1039/C4nj00270a

Huang Y, Liang JJ, Chen YS (2012) The application of graphene based materials for actuators. J Mater Chem 22:3671–3679. doi:10.1039/C2jm15536b

Jung JH, Jeon JH, Sridhar V, Oh IK (2011) Electro-active graphene–Nafion actuators. Carbon 49:1279–1289. doi:10.1016/j.carbon.2010.11.047

Kikuchi K, Tsuchitani S (2009) Nafion®-based polymer actuators with ionic liquids as solvent incorporated at room temperature. J Appl Phys. doi:10.1063/1.3204961

Kim J, Yun S, Ounaies Z (2006) Discovery of cellulose as a smart material. Macromolecules 39:4202–4206. doi:10.1021/Ma060261e

Kim KB, Kim J (2013) Fabrication and characterization of electro-active cellulose films regenerated by using 1-butyl-3-methylimidazolium chloride ionic liquid. Proc Inst Mech Eng C 227:2665–2670. doi:10.1177/0954406213478707

Lee C, Wei XD, Kysar JW, Hone J (2008) Measurement of the elastic properties and intrinsic strength of monolayer graphene. Science 321:385–388. doi:10.1126/science.1157996

Murphy EB, Wudl F (2010) The world of smart healable materials. Prog Polym Sci 35:223–251. doi:10.1016/j.progpolymsci.2009.10.006

Muzart J (2006) Ionic liquids as solvents for catalyzed oxidations of organic compounds. Adv Synth Catal 348:275–295. doi:10.1002/adsc.200505273

Nieto A, Lahiri D, Agarwal A (2012) Synthesis and properties of bulk graphene nanoplatelets consolidated by spark plasma sintering. Carbon 50:4068–4077. doi:10.1016/j.carbon.2012.04.054

Novoselov KS et al (2004) Electric field effect in atomically thin carbon films. Science 306:666–669. doi:10.1126/science.1102896

Ozdemir O, Karakuzu R, Sarikanat M, Akar E, Seki Y, Cetin L, Sen I, Gurses BO, Yılmaz OC, Sever K, Mermer O (2015) Effects of PEG loading on electromechanical behavior of cellulose-based electroactive composite. Cellulose. doi:10.1007/s10570-015-0581-7

Pang JH, Liu X, Zhang XM, Wu YY, Sun RC (2013) Fabrication of cellulose film with enhanced mechanical properties in ionic liquid 1-allyl-3-methylimidaxolium chloride (AmimCl). Materials 6:1270–1284. doi:10.3390/Ma6041270

Patil ML, Sasai H (2008) Recent developments on chiral ionic liquids: design, synthesis, and applications. Chem Rec 8:98–108. doi:10.1002/Tcr.20143

Polu AR, Kumar R (2011) Impedance spectroscopy and FTIR studies of PEG—based polymer electrolytes. J Chem 8:347–353

Polu AR, Kumar R, Causin V, Neppalli R (2011) Conductivity, XRD, and FTIR studies of new Mg^{2+}-ion-conducting solid polymer electrolytes: [PEG: Mg(CH3COO)(2)]. J Korean Phys Soc 59:114–118. doi:10.3938/Jkps.59.114

Qiu XY, Hu SW (2013) "Smart" materials based on cellulose: a review of the preparations, properties, and applications. Materials 6:738–781. doi:10.3390/Ma6030738

Rajkumar T, Ranga Rao G (2008) Characterization of hybrid molecular material prepared by 1-butyl 3-methyl imidazolium bromide and phosphotungstic acid. Mater Lett 62:4134–4136

Ranga Rao G, Rajkumar T, Varghese B (2009) Synthesis and characterization of 1-butyl 3-methyl imidazolium phosphomolybdate molecular salt. Solid State Sci 11:36–42

Ravikiran Y, Kotresh S, Vijayakumari S, Thomas S (2014) Liquid petroleum gas sensing performance of polyaniline-carboxymethyl cellulose composite at room temperature. Curr Appl Phys 14(7):960–964

Sen I et al (2015) Electroactive behavior of graphene nanoplatelets loaded cellulose composite actuators. Compos Part B Eng 69:369–377. doi:10.1016/j.compositesb.2014.10.016

Shahinpoor M, Bar-Cohen Y, Simpson JO, Smith J (1998) Ionic polymer-metal composites (IPMCs) as biomimetic sensors, actuators and artificial muscles—a review. Smart Mater Struct 7:R15–R30. doi:10.1088/0964-1726/7/6/001

Shahinpoor M, Kim KJ (2001) Ionic polymer-metal composites: I. Fundamentals. Smart Mater Struct 10:819–833. doi:10.1088/0964-1726/10/4/327

Shang J, Shao ZZ, Chen X (2008) Electrical behavior of a natural polyelectrolyte hydrogel: chitosan/carboxymethyl-cellulose hydrogel. Biomacromolecules 9:1208–1213. doi:10.1021/Bm701204j

Swatloski RP, Spear SK, Holbrey JD, Rogers RD (2002) Dissolution of cellose with ionic liquids. J Am Chem Soc 124:4974–4975. doi:10.1021/Ja025790m

Wojtoniszak M et al (2012) Synthesis, dispersion, and cytocompatibility of graphene oxide and reduced graphene oxide. Colloids Surf B 89:79–85

Xia JL, Chen F, Li JH, Tao NJ (2009) Measurement of the quantum capacitance of graphene. Nat Nanotechnol 4:505–509. doi:10.1038/Nnano.2009.177

Yang X, He L, Qin S, Tao GH, Huang M, Lv Y (2014) Electrochemical and thermodynamic properties of Ln(III) (Ln = Eu, Sm, Dy, Nd) in 1-butyl-3-methylimidazolium bromide ionic liquid. Plos One. doi:10.1371/journal.pone.0095832

Zare A et al (2011) Ionic liquid 1-butyl-3-methylimidazolium bromide ([Bmim]Br) as a green and neutral reaction media for the catalyst-free synthesis of 1-amidoalkyl-2-naphthols. Sci Iran 18:433–438. doi:10.1016/j.scient.2011.05.005

Zhao Y, Song L, Zhang ZP, Qu LT (2013) Stimulus-responsive graphene systems towards actuator applications. Energy Environ Sci 6:3520–3536. doi:10.1039/C3ee42812e